NeuroImage: Clinical 24 (2019) 101974

Contents lists available at ScienceDirect

NeuroImage: Clinical

journal homepage: www.elsevier.com/locate/ynicl

# Convergence of three parcellation approaches demonstrating cerebellar lobule volume deficits in Alcohol Use Disorder

Edith V. Sullivan[a,*], Natalie M. Zahr[a,b], Manojkumar Saranathan[c], Kilian M. Pohl[a,b], Adolf Pfefferbaum[a,b]

[a] Department of Psychiatry & Behavioral Sciences, Stanford University School of Medicine, Stanford, CA, United States of America
[b] Center for Health Sciences, SRI International, Menlo Park, CA, United States of America
[c] Department of Medical Imaging, University of Arizona, Tucson, AZ, United States of America

ARTICLE INFO

*Keywords:*
Cerebellum
Alcohol
MRI
Cognition
Balance
Nutrition

ABSTRACT

Recent advances in robust and reliable methods of MRI-derived cerebellar lobule parcellation volumetry present the opportunity to assess effects of Alcohol Use Disorder (AUD) on selective cerebellar lobules and relations with indices of nutrition and motor functions. In pursuit of this opportunity, we analyzed high-resolution MRI data acquired in 24 individuals with AUD and 20 age- and sex-matched controls with a 32-channel head coil using three different atlases: the online automated analysis pipeline volBrain Ceres, SUIT, and the Johns Hopkins atlas. Participants had also completed gait and balance examination and hematological analysis of nutritional and liver status, enabling testing of functional meaningfulness of each cerebellar parcellation scheme. Compared with controls, each quantification approach yielded similar patterns of group differences in regional volumes: All three approaches identified AUD-related deficits in total tissue and total gray matter, but only Ceres identified a total white matter volume deficit. Convergent volume differences occurred in lobules I-V, Crus I, VIIIB, and IX. Coefficients of variation (CVs) were < 20% for 46 of 56 regions measured and in general were graded: Ceres < SUIT < Hopkins. The most robust correlations were identified between poorer stability in balancing on one leg and smaller lobule VI and Crus I volumes from the Ceres atlas. Lower values of two essential vitamins—thiamine (vitamin B1) and serum folate (vitamin B9)—along with lower red blood cell count, which are dependent on adequate levels of B vitamins, correlated with smaller gray matter volumes of lobule VI and Crus I. Higher γ-glutamyl transferase (GGT) levels, possibly reflecting compromised liver function, correlated with smaller volumes of lobules VI and X. These initial results based on high resolution data produced with clinically practical imaging procedures hold promise for expanding our knowledge about the relevance of focal cerebellar morphology in AUD and other neuropsychiatric conditions.

## 1. Introduction

The cerebellum is a principal target of central nervous system (CNS) damage related to excessive and chronic consumption of alcohol. Neuropathologically, atrophy is detectable even when cell loss is not; in those cases, cerebellar white matter can exhibit degradation of fiber cores (reviewed by, de la Monte and Tong, 2014; Sutherland et al., 2014). These signs of disrupted fiber integrity have been identified in cases of alcoholism uncomplicated by common concomitants, such as liver cirrhosis or nutritional insufficiencies typically from thiamine depletion causing Wernicke's encephalopathy or Korsakoff's syndrome, although these concomitant complications can exacerbate pathology (Baker et al., 1999; Phillips et al., 1987; Torvik and Torp, 1986; Victor et al., 1989). An early study examining thiamine content and turnover in seven brain structures of thiamine-fed rats and controls identified the cerebellum as exhibiting the highest thiamine content and turnover rate of the regions examined (Rindi et al., 1980).

Neuroradiologically, the mainstay of studies of uncomplicated Alcohol Use Disorder (AUD) concurs with neuropathological findings, which are typically more prominent in white than gray matter (Monnig et al., 2013; Sawyer et al., 2016; Zhao et al., 2019). Quantitative MRI studies report tissue shrinkage typically in the anterior superior vermis, involving regions I-V with additional sites of volume deficits in gray matter (Le Berre et al., 2014; Ritz et al., 2016; Sullivan et al., 2000) and

* Corresponding author at: Department of Psychiatry and Behavioral Sciences, Stanford University School of Medicine (MC5723), 401 Quarry Road, Stanford, CA 94305-5723, United States of America.
*E-mail address:* edie@stanford.edu (E.V. Sullivan).

https://doi.org/10.1016/j.nicl.2019.101974
Received 28 April 2019; Received in revised form 24 July 2019; Accepted 5 August 2019
Available online 07 August 2019

white matter (Sawyer et al., 2016; Sullivan et al., 2000; for review, Zahr and Pfefferbaum, 2017) of the cerebellar hemispheres, also exacerbated by common alcoholism-related concomitant complications (Ritz et al., 2016; Sullivan et al., 2000). Additional alcoholism and lesion studies report selective relations between performance on tasks assessing executive functions (Nakamura-Palacios et al., 2014; Sullivan, 2003; Sullivan et al., 2003), verbal working (Desmond et al., 2003), spatial memory (Chanraud et al., 2010), and learning and Crus I, Crus II, and lobule VI volumes (Schmahmann, 2019; Stoodley et al., 2016; Stoodley et al., 2012), whereas tests of gait and upright postural stability are often related to volumes of the anterior superior (I-IV) (Sullivan et al., 2000; Sullivan et al., 2006) and floccular-nodular (IX/X) lobules (Angelaki et al., 2010) unless cognitive information processing speed is also considered with gait speed (Nadkarni et al., 2014). By contrast, cerebellar volume shrinkage in normal aging occurs more inferiorly and posteriorly, in vermian lobules VI-X (Raz et al., 1998), Crus I-II and vermian lobules VI and VIIA (Yu et al., 2017), and lobules V-VI (Ziegler et al., 2012). Thus, alcoholics who continue to drink or initiate dependent drinking later in life (cf., Breslow et al., 2017; Sullivan et al., 2018) are at heightened risk for developing widespread cerebellar volume deficits with ramifications for cerebellar-based performance deficits.

Recognition of local differences in regional cerebellar degradation in AUD, normal aging, and other neuropsychiatric conditions (e.g., Koeppen, 2018; Mosconi et al., 2015; Schmahmann, 2019) emphasizes the relevance of considering focal lobular and tissue analysis. Despite this need, measurement of individual lobules and segmentation of their tissue compartments have been challenging because of complexity of the fine branching of cerebellar folia that results in partial voluming of imaging data, that is, mixing of tissue types in acquired voxels. Consequently, a number of methods have been devised to address regional cerebellar quantification with varying success (e.g., Price et al., 2014). A rigorous comparison of five approaches with practical computational burdens— SUIT (Spatially Unbiased Infra-Tentorial template) (Diedrichsen et al., 2009), MAGeT (Chakravarty et al., 2013; Park et al., 2014), RASCAL (Weier et al., 2014), Ceres (CEREbellum Segmentation) (Manjon and Coupe, 2016), and manual delineation— identified Ceres as the most robust and reliable method of the five tested for volumetry of gray matter in 12 cerebellar lobules (Carass et al., 2018; Romero et al., 2017).

The current study used three different quantification approaches, each with its own published atlas: Ceres (Manjon and Coupe, 2016), SUIT (Diedrichsen et al., 2009), and the Johns Hopkins atlas (Yang et al., 2016). Participants were men and women with AUD or unaffected controls who had undergone high-resolution, structural MRI acquired with a 32-channel head coil (Zahr et al., 2019). These data had sufficient resolution and low noise amenable to automated tissue segmentation and regional cerebellar parcellation with each approach. Herein, we tested the following hypotheses: 1) Relative to controls, the AUD group would exhibit gray matter volume deficits in lobules I-V, VIIB, IX, and Crus I evident with all three analysis approaches, but with an open-ended question regarding the relative power of each approach to detect differences; 2) correlations between performance on gait and balance testing and lobular volumes would suggest functional relevance of regional volumes; and 3) further exploratory correlations between hematological indices of nutrition and liver function and lobular volumes would suggest relevance to alcoholism-related factors and ability of each atlas to show these relations.

## 2. Material and methods

### 2.1. Participants

MRI data were available for 24 alcoholics (17 men, 7 women) and 20 controls (13 men, 7 women), age 39 to 74 years (Zahr et al., 2019). As stated previously (Zahr et al., 2019) and summarized next, all participants provided written informed consent to partake in this study, which was conducted with the approval of the Institutional Review Boards of Stanford University and SRI International. Participants received a stipend of $200 for completing the study.

All but 2 control participants underwent interviews with the Structured Clinical Interview for DSM-IV revised by research clinicians in our laboratory to determine eligibility for the study and for MRI scanning. Interviews also included structured health questionnaires, a semi-structured timeline follow-back interview to quantify lifetime alcohol consumption (Skinner, 1982; Skinner and Sheu, 1982), and the Clinical Institute Withdrawal Assessment for Alcohol (CIWA). Subjects were excluded for significant history of medical (e.g., epilepsy, stroke, multiple sclerosis, uncontrolled diabetes, or loss of consciousness > 30 min), psychiatric (i.e., schizophrenia or bipolar I disorder), or neurological disorders (e.g., neurodegenerative disease).

Each participant also underwent a blood draw and a neuropsychological test battery. Blood samples (~40 cc) were collected and analyzed by Quest Diagnostics for complete blood count with differential, comprehensive metabolic panel, and human immunodeficiency virus (HIV) and hepatitis C (HCV) screening, which identified 2 controls and 4 AUD subjects to be seropositive for hepatitis C virus (HCV) infection.

The total lifetime alcohol consumption of the AUD group was > 30 times that of the controls. Further, the AUD group had fewer years of education, had lower socioeconomic status, and endorsed more depressive symptoms than the controls. Compared with controls, more AUD participants were African American and were cigarette smokers. Group demographic and hematological descriptive statistics appear in Table 1.

Of the 24 alcoholics, 9 (37.5%) had a lifetime history of Major Depressive Disorder; however, all nine were in remission at the time of assessment, and none had current depression. In addition, 12 alcoholics (50.0%) had a lifetime history of an anxiety disorder; 10 or the 12 had a current anxiety disorder. Further, 18 alcoholics had a lifetime history of

**Table 1**
Characteristics of the study groups: mean ± SD / frequency count.

| | Control ($n$ = 20) | AUD ($n$ = 24) | $p$-Value* |
|---|---|---|---|
| N (men/women) | 13 / 7 | 17 / 7 | 0.68 |
| Age (years) | 54.1 ± 9.3 | 53.7 ± 8.8 | 0.90 |
| Handedness (right/left) | 19 / 1 | 20 / 4 | 0.23 |
| Ethnicity[a] (Caucasian/ African American/ Asian) | 8 / 5 / 7 | 14 / 9 / 1 | **0.03** |
| Body Mass Index | 25.0 ± 3.6 | 28.9 ± 5.7 | **0.01** |
| Education (years) | 16.2 ± 2.3 | 13.0 ± 1.8 | **0.0001** |
| Socioeconomic status[b] | 25.4 ± 15.7 | 44.5 ± 13.2 | **0.0001** |
| Beck Depression Index (BDI) | 5.2 ± 5.2 | 14.7 ± 10.0 | **0.001** |
| AUD onset age | – | 21.7 ± 6.6 | n.a. |
| Days since last drink | – | 105.7 ± 94.5 | n.a. |
| Lifetime alcohol consumption (kg) | 53.6 ± 81.2 | 1798.3 ± 1638.0 | < **0.0001** |
| Alcohol consumption years | – | 32.0 ± 9.6 | n.a. |
| CIWA score | – | 23.2 ± 17.7 | n.a. |
| Smoker (never/past/ current) | 18 / 0 / 2 | 4/6/2014 | **0.0001** |
| Nicotine (daily) | 1.1 ± 3.3 | 4.6 ± 3.9 | **0.008** |
| Hematological Indices | | | |
| Red blood count (RBC) | 4.90 ± 0.54 | 4.62 ± 0.39 | 0.066 |
| Whole blood thiamine (B1) | 111.4 ± 23.7 | 123.0 ± 31.8 | 0.295 |
| Folate (B9) | 14.9 ± 5.0 | 16.0 ± 6.3 | 0.557 |
| Cobalamins (B12) | 482.2 ± 171.1 | 570.1 ± 240.6 | 0.201 |
| γ-Glutamyl transferase (GGT) | 20.9 ± 13.5 | 38.0 ± 35.3 | 0.058 |

*t*-Tests used on continuous variables (e.g., age); |2 used on nominal variables (e.g., handedness).
**Bold** = statistically significant at p ≤ .05 (2-tailed).
[a] Self-defined.
[b] Lower score = higher status.

DSM-IV substance abuse/dependence, but all 18 were in remission (remission range = 9 to 2099 weeks, mean ± SD = 515.7 ± 728.8 weeks; median = 70 weeks. The most common substance of abuse was cocaine, occurring in 12 of the 18 with substance abuse/dependence.

### 2.2. MRI acquisition parameters

MRI structural data were acquired in the sagittal plane on a 3 T General Electric (GE) Discovery MR750 (GE Healthcare Systems, Waukesha, MI) with an Array Spatial Sensitivity Encoding Technique (ASSET) for parallel and accelerated imaging with a 32-channel head coil (Nova Medical, Wilmington, MA) (Zahr et al., 2019).

T1-weighted scans were cerebral spinal fluid (CSF)-nulled Magnetization Prepared Rapid Gradient echo (MPRAGE) acquired with the following parameters: TR = 8 ms, TE = 3.5 ms, TI = 1100 ms, TS (i.e., time between two successive inversion pulses) = 3.0 s, Flip Angle = 9, FOV = 18 cm, matrix = 200 × 200, thick = 1 mm, slices = 210 slices, resolution = 0.9 × 0.9 × 1.0.

T2-weighted scans were 3D fast spin-echo with variable refocusing flip angle (T2 Cube) and acquired with the following parameters: Fat Sat = ON, TR = 3500 ms, Effective TE = 62 ms, Echo Train Length (ETL) = 84, FOV = 18 cm, matrix = 224 × 224, thick = 1 mm, slices = 210, resolution = 0.8 × .08 × 1.0. Acquisition extended from ear to ear and from the top of scalp to the base of cerebellum.

The T1-weighted scans yielded excellent gray/white tissue conspicuity, and the T2 scans provided full information about brain volume, especially when cortical and cerebellar tissue shrinkage is replaced by CSF, as occurs in disorders such as AUD.

### 2.3. MRI analysis

The T1-weighted (T1w) and T2-weighted (T2w) MRIs of each participant were first processed via our laboratory pipeline (Pfefferbaum et al., 2018a) using FreeSurfer 6.0. Preprocessing of the T1w and T2w MRI data involved noise removal (Coupe et al., 2008), correcting field inhomogeneity using N4ITK (Tustison et al., 2011), aligning T2w to T1w MRIs using CMTK (Rohlfing and Maurer, 2003), repeating image inhomogeneity correction of both modalities confined to the brain mask defined by aligning SRI24 atlas (Rohlfing et al., 2010) to T1w MRI using the symmetric, diffeomorphic non-rigid registration called ANTS (Klein et al., 2009). The brain mask was refined with FSL BET (Smith, 2002) applied to bias corrected T2w images. Using the refined masked, we repeated the image inhomogeneity correction. Whole brain imaging enabled quantification of the total intracranial volume (ICV) to serve as control for normal variation in headsize (Mathalon et al., 1993; Pfefferbaum et al., 1992).

### 2.4. Cerebellar parcellation of lobular gray matter volumes

#### 2.4.1. Ceres

Cerebellar segmentation was accomplished with Ceres (Carass et al., 2018; Manjon and Coupe, 2016; Romero et al., 2017). T1 data were uploaded and retrieved from [http://volbrain.upv.es]. Data comprised left and right measures of the whole cerebellum volume and gray matter, and 12 lobules (I + II, III, IV, V, VI, Crus I, Crus II, VIIB, VIIIA, VIIIB, IX, X). For comparison with SUIT output, we summed the volumes of I to IV; for comparison with Hopkins output, we summed the volumes of lobules I to V. Cerebellar volume of the total white matter was determined from the difference between whole volume and whole gray matter volume. In-house software extracted volumetric data from the downloaded Ceres result tables; pdf rendering of Ceres fits were inspected for quality, and all images were acceptable. Included in the Ceres downloads were estimates of SNR and ICV. Only data with SNR > 20 were considered usable. Our 32-channel MRI data surpassed the recommendation with SNR ranging from 22.7 to 89.8 across the two groups (AUD mean = 48.7; control mean = 56.2). The ICV from T2-weighted masking was used because CSF-nulled T1 scan produced too vigorous skull stripping via Ceres. Fig. 1 displays an example segmentation and parcellation of regions from a single case. Fig. 2 displays plots of total cerebellar tissue, gray matter, and white matter for each analysis approach.

#### 2.4.2. SUIT

This atlas enabled identification and volumetry of total cerebellar tissue, gray matter, and white matter. Regional parcellation yielded volumes of 10 lobules: I-IV, V, VI, Crus I, Crus II, VIIB, VIIIA, VIIIB, IX, and X (Fig. 1B). The software is an open-source SPM toolbox [http://www.diedrichsenlab.org/imaging/propatlas.htm] (Diedrichsen et al., 2009) and was applied to the skull-stripped and inhomogeneity-corrected T1 data.

#### 2.4.3. Johns Hopkins atlas

Implementation of this atlas required the cerebellum to be preprocessed with FreeSurfer (V5.3) (Fischl et al., 2002) and then parcellelated by the Hopkins software tool (Yang et al., 2016), which combines multi-atlas segmentation with the graph-cut algorithm and random forest. The software tool uses an atlas consisting of 15 manually generated segmentations (Yang et al., 2016), each identifying 25 cerebellar regions, including unilateral hemisphere measures (Fig. 1B). For comparison across the three analysis approaches herein, we used bilateral volumes of three global measures (total tissue, gray matter, and white matter) and 8 bilateral hemisphere measures (I-V, VII, Crus I, Crus II, VIIB, VIII, IX, and X).

### 2.5. Cognitive and postural stability testing

Participants completed a neuropsychological battery to assess current levels of general cognitive and performance abilities. The Wechsler Test of Adult Reading (WTAR) (Wechsler, 2001) estimated a premorbid intelligence quotient (IQ). The Montreal Cognitive Assessment (MoCA) battery (Nasreddine et al., 2005) provided a measure of current general cognitive capacity.

Ataxia testing (Fregly et al., 1972; Sullivan et al., 2000) was conducted under the following conditions, first with eyes open and then for another set of trials with eyes closed: stand heel-to-toe (60 s/trial), stand on one foot (30 s/trial for each foot); and walk a line for a maximum of 10 steps. Each condition was conducted twice unless a maximum score was achieved on the first trial; then by default the score would be the maximum for two trials (e.g., 60 s for trial 1 of standing heel-to-toe would result in the maximum (best) score of 120 s). Scores from each of the 8 conditions were expressed as *Z*-scores standardized for age based on the controls.

### 2.6. Statistical analysis

The mainstay of statistical analysis was performed using R 3.5.1 (R Core Team, 2019) on bilateral volumes, which were the sums of left and right regional volumes. The R code is provided in Supplemental Material. Separate linear models (*lm)* were constructed predicting the volume of described each lobule from sex, ICV, and age, for the diagnostic and control groups separately. This process was applied for volumes obtained using Ceres, Hopkins, and SUIT, and each regional volume was analyzed separately. For more intuitive graphical presentation, group means were added to the residuals. Group differences were determined by *t*-tests, which were considered significant at $p = .05$ (2-tailed). In addition, we tested for diagnosis-by-age and diagnosis-by-sex interactions.

Coefficients of variation (CVs) were calculated (SD/mean) for each regional volume for each measurement approach and for each subject group to index, without the need for scalar equivalence, variation in the distributions of regional volumes for a volume's mean. Smaller CVs

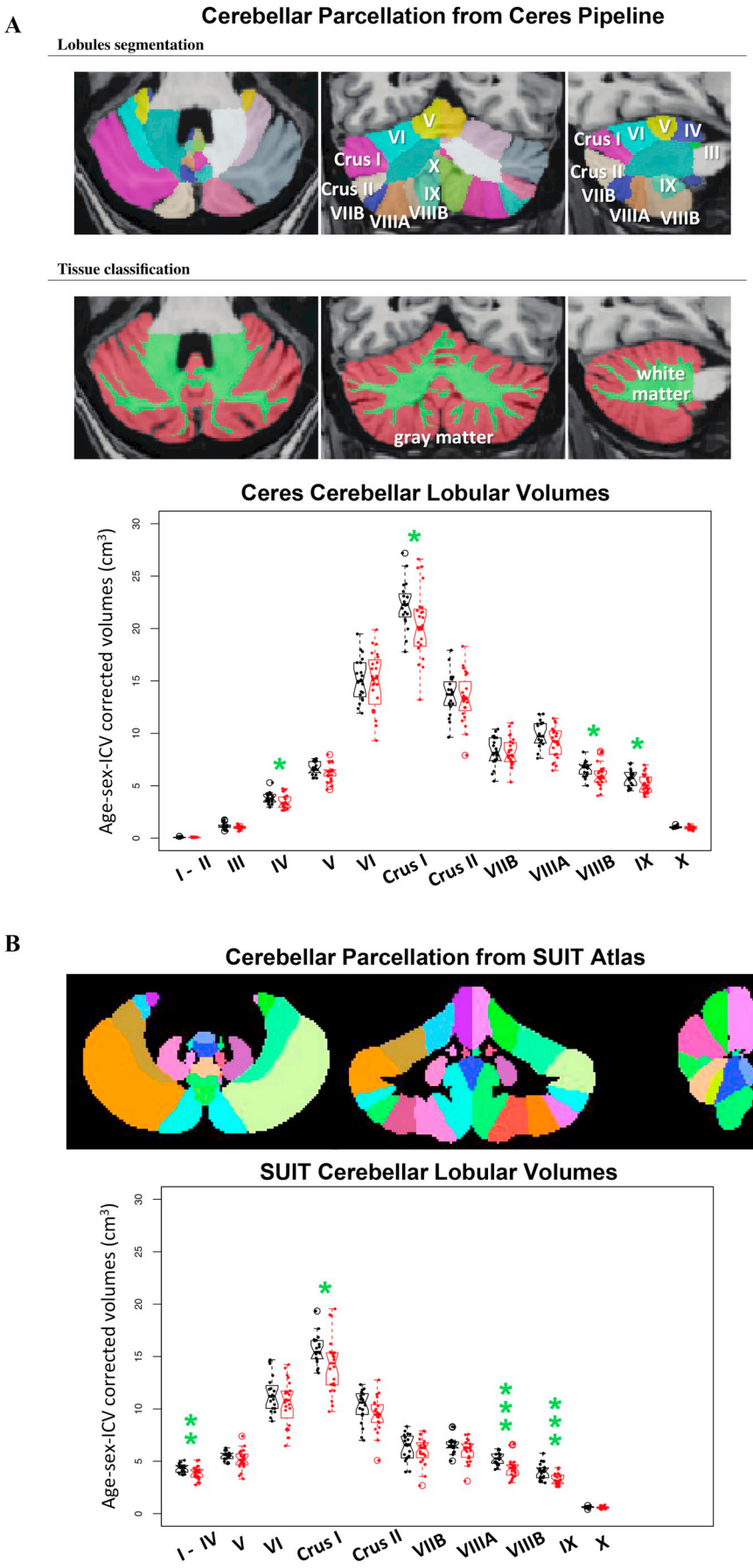


(caption on next page)

**Fig. 1.** A. An example of volBrain/Ceres cerebellum output of quantification of a 58 year-old control woman from our study. The top row of images demonstrates the quality of the lobules parcellation. Lobules V-X are visible on the middle (coronal) slice and lobules III-IX are visible on the right (sagittal) slice; the left (axial) slice is not labeled. The bottom row of images displays the gray-white tissue classification of the three planes. The violin plots display the regional gray matter volumes (adjusted for age, sex, and ICV with the mean added back in for display) of the 12 Ceres parcellations of the controls (black) and alcoholics (red).
*p ≤ .05, **p ≤ .01, ***p < .001. B. Top half: The SUIT atlas parcellation in axial, coronal, and sagittal planes. The violin plots below the images display the regional gray matter volumes (adjusted for age, sex, and ICV with the mean added back in for display) of the 10 SUIT parcellations of the controls (black) and alcoholics (red).
Bottom half: An example of the Johns Hopkins atlas parcellation in axial, coronal, and sagittal planes of a participant our study. The violin plots below the images display the regional gray matter volumes (adjusted for age, sex, and ICV with the mean added back in for display) of the 8 Hopkins lobule parcellations of the controls (black) and alcoholics (red).
*$p \leq .05$, **$p \leq .01$, ***$p < .001$.

indicate less variation in volumes and have been considered a measure of precision or repeatability.

Pearson correlations tested relations between cerebellar lobular volumes and ataxia scores, alcohol history measures, and hematological values. All correlations with $p \leq .05$ are reported and those meeting family-wise Bonferroni correction (1-tailed) and False Discovery Rate (FDR) correction.

## 3. Results

### 3.1. Group differences in cerebellar lobular volumes

Means ± standard deviations (SD) for each cerebellar measure for each quantification approach by group are presented in Table 2 and Figs. 1A and B; values for each region measured with each quantification approach are provided in Supplemental Material. Also presented are statistical results for group comparisons using the *lm* to account for variance attributed to normal age, ICV, and sex. Color coding of Table 2 values indicates two approaches for determining statistical significance between groups: nominal values of uncorrected p ≤ .05 (bold black font for individual comparisons and bold red font for regions meeting p ≤ .05 with two quantification methods) and yellow highlighting for volumes meeting FDR correction for $p \leq .05$.

Compared with controls, the AUD group had smaller volumes of the total cerebellum, total gray matter, and total white matter. All three were significant with FDR correction for Ceres, and total tissue and gray matter were significant with FDR for SUIT and Hopkins volumes.

Regional analysis of cerebellar gray matter revealed FDR-corrected volume deficits in the AUD group relative to the control group as follows: Ceres lobules I-IV and I-V, Crus I, VIIIB, and IX; SUIT lobules I-IV, VIIIB, and IX; and Hopkins lobules I-V, Crus II, and IX (Fig. 1A and B). Neither group-by-age nor group-by-sex interactions were significant for any lobule for any method.

Next, we used the CV as a unit-less index of precision of each measurement (Table 3). Not surprisingly, total cerebellar and gray matter volumes, which were the largest measures, had the smallest CVs and produced group differences by all three measurement approaches. Lobules I-II, III, and IV had high CVs with Ceres, ranging from 14.0% to 52.4%. Adding lobules I-IV and I-V volumes of Ceres to match, at least nominally, the SUIT and the Hopkins atlases substantially reduced the score dispersion and brought the CVs into line across the three measurement approaches, with CVs now ranging from 8.3% to 16.9%. Of 56 regional measures, 46 had CV ≤ 20%, 9 had CVs ranging between 20.4% to 23.3%, and only one exceeded this range and was 47.2% for Hopkins lobule X (Table 3). In general, regions with lower CVs were more likely to produce group differences.

### 3.2. Group differences in neuropsychological test performance

The WTAR estimated IQ and indicated that the AUD group achieved

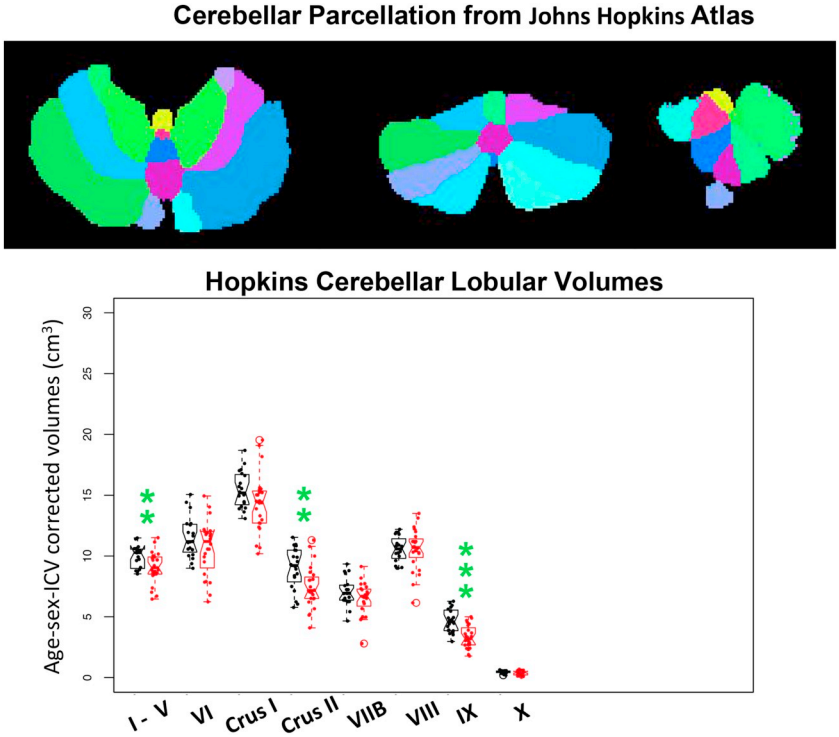


**Fig. 1.** (*continued*)

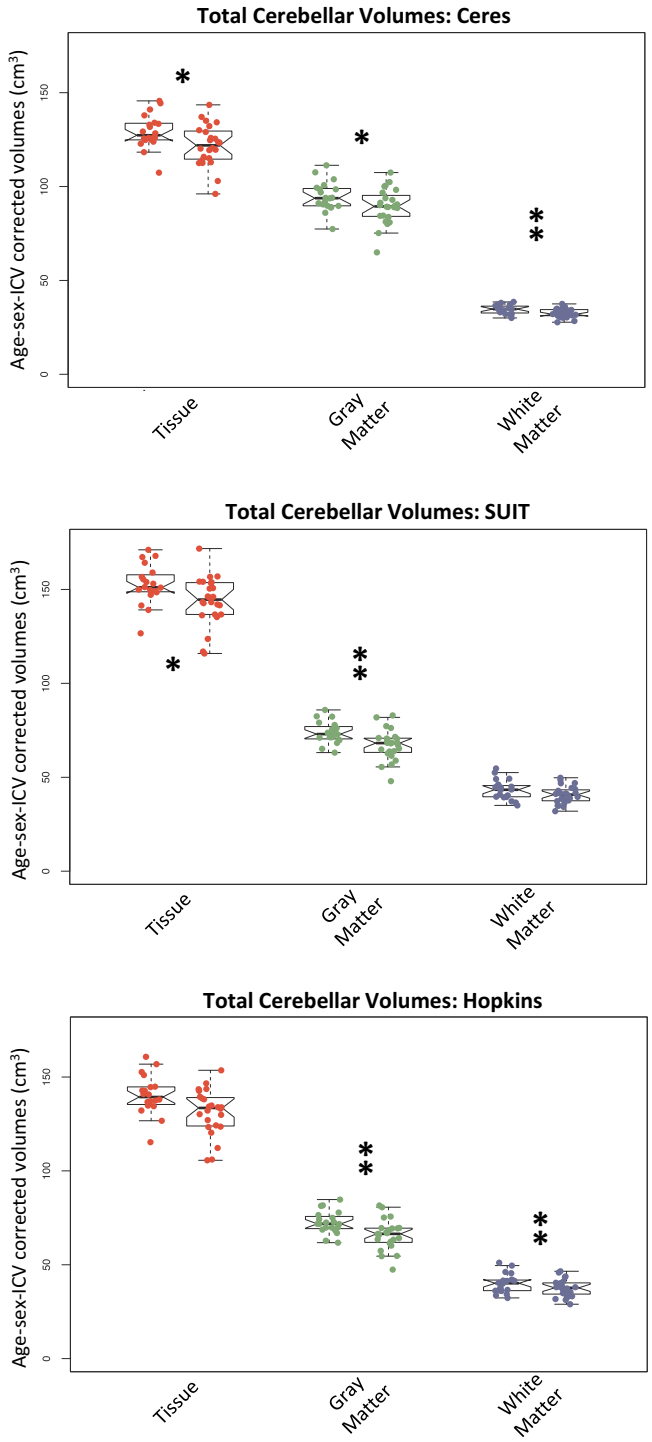


**Fig. 2.** The violin plots of total cerebellum tissue, total gray matter, and total white matter volumes (adjusted for age, sex, and ICV with the mean added back in for display) quantified with the three analysis approaches: Ceres (top), SUIT (middle), and Hopkins (bottom). The control values are the left of a color pair and the AUD values are the right of a pair. *p ≤ .05, **p ≤ .01.

significantly lower scores than controls. Although no AUD participant was clinically demented, the alcoholics as a group achieved significantly poorer scores on the MoCA battery (Table 4).

Each ataxia score was adjusted for variance associated with age estimated from control performance; means ± SDs are presented in Table 4. The AUD group was mildly to moderately impaired on three of the four ataxia conditions with eyes open: walk heel-to-toe (−0.74 SD below normal), stand on left leg (−0.71 SD below normal), and stand on right leg (−0.98 SD below normal).

### 3.3. Correlations with cerebellar volumes in AUD: ataxia scores

Poorer ability to stand on one leg with eyes open correlated with smaller volumes of lobule VI of all three atlases. In addition, left leg balance performance correlated with smaller Crus I volumes by Ceres and smaller lobule X volumes by SUIT (Table 5 and Fig. 3).

### 3.4. Correlations with cerebellar volumes in AUD: hematological values

Again, correlations with lobule VI volumes occurred most regularly across the three quantification approaches. In general, lower red blood count, serum folate, and whole blood thiamine levels and higher GGT levels correlated with smaller VI volumes (Table 5 and Fig. 4). Higher GGT levels were also related to smaller lobule X volumes of Ceres and SUIT.

### 3.5. Correlations with cerebellar volumes in AUD: alcohol history measures

None of the cerebellar volumes of any quantification method correlated with amount of alcohol drunk in a lifetime. By contrast, older age at onset of an AUD diagnosis was predictive of smaller volumes of Ceres lobule VIIB and Crus II, SUIT lobules V and VIIB, and Hopkins lobules

I-V and VIIB despite use of age-corrected brain volumes (Table 5 and Fig. 5).

A series of multiple regression analyses conducted with Statview was used to discern the separate contributions of age and AUD onset age to regional cerebellar volumes. Accordingly, for the Ceres relations, age when first diagnosed with alcohol dependence was the significant contributing factor to Ceres lobule VIIB volumes (onset age $p = .007$; current age $p = .855$) and Crus II volumes (onset age $p = .0024$; current age $p = .328$) over and above current age. Similarly for SUIT, onset age was the significant contributing factor to lobule V volumes (onset age $p = .021$; current age $p = .120$) and VIIB volumes (onset age $p = .031$; current age $p = .696$) over and above current age. For the Hopkins approach, onset age was the significant contributing factor to lobule composite I-V volumes (onset age $p = .011$; current age $p = .083$) and VIII volumes (onset age $p = .062$; current age $p = .884$) over and above current age.

## 4. Discussion

Primary aims for implementing and comparing multiple analysis approaches for quantification of individual cerebellar lobules were to determine convergence in their success of identifying patterns of gray matter volume deficits and behavioral and hematological correlates of regional volumes in AUD. Accordingly, taken from neuropathological reports and earlier neuroimaging studies that used grosser measures of the cerebellum, we tested the hypothesis that the AUD group would have significantly smaller gray matter volumes than controls in lobules I-IV, VIIB, IX, and Crus I regardless of quantification procedure used. In partial support of our prediction, we found modest volume deficits in total gray matter and lobule IX with all three methods. In addition, Ceres and SUIT identified regional volume deficits in lobules I-IV, Crus I, and VIIIB; Ceres and Hopkins identified deficits in lobule I-V. Only the Hopkins approach identified a volume deficit in Crus II. Thus the pattern of regional group differences was similar with the Ceres and SUIT methods and different from that found with the Hopkins method. Reasons for these differences may be due to parcellation schemes; for example, the Hopkins method distinguishes regions assigned to the vermis that might be included in hemispheric lobular volumes in Ceres and SUIT. Further, the average CVs of the Ceres (13.9%) and SUIT (15.8%) methods (cf., Carass et al., 2018) were lower than those of the

**Table 2**
Cerebellar volumes by tissue type and region for 3 analysis approaches: mean (SD) volumes adjusted for ICV, sex, and age with linear regression.

| | CERES | | Welch 2 sample | | SUIT | | Welch 2 sample | | Hopkins | | Welch 2 sample | |
|---|---|---|---|---|---|---|---|---|---|---|---|---|
| Regional Volumes | Control mean ($cm^3$) | AUD mean ($cm^3$) | t | p | Control mean ($cm^3$) | AUD mean ($cm^3$) | t | p | Control mean ($cm^3$) | AUD mean ($cm^3$) | t | p |
| Total Tissue | 129.244 | 121.916 | 2.451 | 0.019 | 152.572 | 143.955 | 2.459 | 0.018 | 140.349 | 131.302 | 2.687 | 0.010 |
| | (8.944) | (10.889) | | | (10.421) | (12.823) | | | (10.285) | (12.052) | | |
| Total Gray Matter | 94.643 | 89.364 | 2.046 | 0.047 | 73.803 | 67.210 | 3.174 | 0.003 | 72.507 | 65.899 | 3.164 | 0.003 |
| | (7.784) | (9.333) | | | (5.714) | (8.023) | | | (5.887) | (7.946) | | |
| Total White Matter | 34.601 | 32.552 | 2.851 | 0.007 | 43.296 | 40.576 | 1.812 | 0.078 | 40.051 | 37.489 | 1.741 | 0.090 |
| | (2.330) | (2.426) | | | (5.242) | (4.595) | | | (5.109) | (4.547) | | |
| Lobule Gray Matter | | | | | | | | | | | | |
| I-II | 0.082 | 0.078 | 0.309 | 0.760 | — | — | — | — | — | — | — | — |
| | (0.043) | (0.024) | | | | | | | | | | |
| III | 1.152 | 1.006 | 2.044 | 0.049 | — | — | — | — | — | — | — | — |
| | (0.276) | (0.176) | | | | | | | | | | |
| IV | 3.813 | 3.439 | 2.079 | 0.044 | — | — | — | — | — | — | — | — |
| | (0.536) | (0.657) | | | | | | | | | | |
| I-IV | 5.046 | 4.523 | 2.570 | 0.014 | 4.325 | 3.879 | 2.892 | 0.006 | — | — | — | — |
| | (0.581) | (0.767) | | | (0.410) | (0.608) | | | | | | |
| I-V | 11.705 | 10.809 | 2.572 | 0.014 | — | — | — | — | 9.961 | 9.070 | 2.686 | 0.010 |
| | (0.977) | (1.330) | | | | | | | (0.903) | (1.289) | | |
| V | 6.659 | 6.286 | 1.784 | 0.082 | 5.511 | 5.146 | 1.764 | 0.087 | | | — | — |
| | (0.606) | (0.780) | | | (0.416) | (0.906) | | | | | | |
| VI | 15.129 | 15.030 | 0.137 | 0.892 | 11.406 | 10.608 | 1.393 | 0.171 | 11.516 | 10.676 | 1.421 | 0.163 |
| | (2.047) | (2.723) | | | (1.729) | (2.071) | | | (1.658) | (2.254) | | |
| Crus I | 22.248 | 20.429 | 2.203 | 0.033 | 15.661 | 14.130 | 2.454 | 0.019 | 15.441 | 14.316 | 1.907 | 0.064 |
| | (2.205) | (3.244) | | | (1.399) | (2.644) | | | (1.489) | (2.385) | | |
| Crus II | 13.657 | 13.326 | 0.512 | 0.611 | 10.242 | 9.426 | 1.724 | 0.092 | 8.989 | 7.418 | 2.994 | 0.005 |
| | (1.992) | (2.296) | | | (1.535) | (1.597) | | | (1.739) | (1.727) | | |
| VIIB | 8.264 | 8.224 | 0.098 | 0.923 | 6.297 | 6.010 | 0.746 | 0.460 | 7.066 | 6.499 | 1.515 | 0.137 |
| | (1.383) | (1.315) | | | (1.259) | (1.286) | | | (1.153) | (1.328) | | |
| VIIIA | 9.902 | 9.162 | 1.864 | 0.069 | 6.567 | 6.017 | 2.039 | 0.048 | — | — | — | — |
| | (1.215) | (1.418) | | | (0.754) | (1.032) | | | | | | |
| VIIIB | 6.6095 | 5.9358 | 2.543 | 0.015 | 5.249 | 4.309 | 4.165 | 0.000 | — | — | — | — |
| | (0.713) | (1.037) | | | (0.586) | (0.899) | | | | | | |
| VIII | — | — | — | — | — | — | — | — | 10.553 | 10.528 | 0.062 | 0.951 |
| | | | | | | | | | (1.049) | (1.701) | | |
| IX | 5.758 | 5.175 | 2.256 | 0.029 | 4.009 | 3.281 | 3.644 | 0.001 | 4.656 | 3.325 | 4.595 | 0.000 |
| | (0.840) | (0.869) | | | (0.737) | (0.554) | | | (0.970) | (0.941) | | |
| X | 1.043 | 0.995 | 1.240 | 0.223 | 0.621 | 0.577 | 1.461 | 0.152 | 0.462 | 0.384 | 1.780 | 0.083 |
| | (0.096) | (0.158) | | | (0.083) | (0.118) | | | (0.108) | (0.181) | | |

Hopkins (20.3%) method, potentially contributing to differences in measurement repeatability or precision.

The anterior deficits would be predicted from other studies of alcoholism, and the posterior and inferior regions would be predicted from a recent analysis of the corpus medullare. Specifically, use of a novel Jacobian deformation morphology approach to quantify the total corpus medullare of the cerebellum revealed AUD-related volume deficits and accelerated aging in the total corpus medullare and regional shrinkage of surfaces adjacent to lobules I-V, IX, and X (Zhao et al., 2019).

When aging is compounded with AUD, controlled studies of cortical tissue have identified age-alcoholism interactions, where age-related

**Table 3**
Coefficients of variation (CV) for each measurement approach.

| | Ceres CV | | SUIT CV | | Hopkins CV | |
|---|---|---|---|---|---|---|
| Regional Volumes | Control | AUD | Control | AUD | Control | AUD |
| Total Tissue | 6.9% | 8.9% | 6.8% | 8.9% | 7.3% | 9.2% |
| Total Gray Matter | 8.2% | 10.4% | 7.7% | 11.9% | 8.1% | 12.1% |
| Total White Matter | 6.7% | 7.5% | 12.1% | 11.3% | 12.8% | 12.1% |
| Lobule Gray Matter | | | | | | |
| I-II | 52.4% | 31.1% | — | — | — | — |
| III | 23.9% | 17.5% | — | — | — | — |
| IV | 14.0% | 19.1% | — | — | — | — |
| I-IV | 11.5% | 17.0% | 9.5% | 15.7% | — | — |
| I-V | 8.3% | 12.3% | | | 9.1% | 14.2% |
| V | 9.1% | 12.4% | 7.6% | 17.6% | | |
| VI | 13.5% | 18.1% | 15.2% | 19.5% | 14.4% | 21.1% |
| Crus I | 9.9% | 15.9% | 8.9% | 18.7% | 9.6% | 16.7% |
| Crus II | 14.6% | 17.2% | 15.0% | 16.9% | 19.3% | 23.3% |
| VIIB | 16.7% | 16.0% | 20.0% | 21.4% | 16.3% | 20.4% |
| VIIIA | 12.3% | 15.5% | 11.5% | 17.1% | — | — |
| VIIIB | 10.8% | 17.5% | 11.2% | 20.9% | — | — |
| VIII | — | — | — | — | — | — |
| IX | 14.6% | 16.8% | 18.4% | 16.9% | 20.8% | 28.3% |
| X | 9.2% | 15.8% | 13.4% | 20.4% | 23.3% | 47.2% |

**Table 4**
Mean ± SD score on neuropsychological tests.

| | Control | AUD | *t*-Value | p-Value* | Cohen's d |
|---|---|---|---|---|---|
| WTAR IQ (scaled score) | 106.6 ± 13.74 | 93.9 ± 14.36 | 2.850 | **0.007** | 0.906 |
| MoCA | 26.0 ± 3.16 | 23.5 ± 2.34 | 3.030 | **0.004** | 0.899 |
| Ataxia: Eyes Open | | | | | |
| Stand heel-to-toe | −0.019 ± 1.031 | −0.274 ± 1.153 | 0.724 | 0.474 | 0.077 |
| Walk heel-to-toe | −0.018 ± 1.041 | −0.738 ± 1.012 | 2.185 | **0.035** | 0.544 |
| Stand on left leg | −0.009 ± 1.027 | −0.709 ± 1.022 | 2.124 | **0.040** | 0.683 |
| Stand on right leg | −0.012 ± 1.031 | −0.984 ± 1.006 | 2.973 | **0.005** | 0.954 |
| Ataxia: Eyes Closed | | | | | |
| Stand heel-to-toe | 0.000 ± 1.032 | −0.045 ± 1.069 | 0.136 | 0.893 | 0.043 |
| Walk heel-to-toe | 0.001 ± 1.019 | 0.275 ± 2.139 | −0.498 | 0.622 | 0.164 |
| Stand on left leg | −0.014 ± 1.010 | −0.430 ± 0.640 | 1.558 | 0.128 | 0.492 |
| Stand on right leg | −0.010 ± 1.017 | −0.398 ± 0.650 | 1.440 | 0.158 | 0.452 |

* Bold font indicates difference at the 0.05 level (2-tailed).

**Table 5**
Correlations between regional cerebellar volumes and balance scores and hematological indices.

| | Ceres | r | p | Rho | p | SUIT | r | p | Rho | p | Hopkins | r | p | Rho | p |
|---|---|---|---|---|---|---|---|---|---|---|---|---|---|---|---|
| **Ataxia: Eyes Open** | | | | | | | | | | | | | | | |
| **Stand on left leg** | VI | .447 | **.043*** | .409 | .068 | VI | .452 | **.040** | .431 | .054 | VI | .437 | **.047** | .397 | 0.076 |
| | Crus I | .472 | **.031*** | .457 | **.041** | X | .492 | **.024** | .522 | **.020** | | | | | |
| **Stand on right leg** | VI | .497 | **.022*** | .433 | .053 | VI | .458 | **.037** | .369 | .099 | VI | .495 | **.023** | .412 | 0.065 |
| **Hematological Indices** | | | | | | | | | | | | | | | |
| **Red blood count (RBC)** | VI | .498 | **.018*** | .416 | .057 | VI | .425 | .049 | .232 | .287 | VI | 0.414 | .055 | 0.291 | 0.182 |
| **Whole blood thiamine (B1)** | VI | .586 | **.005*** | .603 | **.007** | VI | .614 | **.003*** | .581 | **.009** | VI | 0.610 | **.003*** | 0.585 | **0.009** |
| | | | | | | | | | | | VIII | 0.458 | **.037** | 0.497 | **0.026** |
| **Serum folate (B9)** | VI | .555 | **.009*** | .532 | **.017** | VI | .417 | .060 | .251 | .262 | VI | 0.418 | .060 | 0.333 | 0.137 |
| | Crus I | .458 | **.037*** | .455 | **.042** | | | | | | | | | | |
| **γ-glutamyl transferase (GGT)** | VI | -.479 | **.024*** | -.455 | **.037** | VI | -.482 | **.023** | -.453 | **.038** | I-V | -0.458 | **.032** | -0.246 | 0.260 |
| | X | -.509 | **.015*** | -.262 | .230 | X | -.444 | **.038** | -.343 | .116 | VI | -0.422 | .051 | -0.304 | 0.164 |
| **Age of AUD Onset** | Crus II | -.577 | **.003*** | -.617 | **.003** | V | -.406 | **.049** | -.535 | **.010** | I-V | -0.436 | **.033** | -0.436 | **0.037** |
| | VIIB | -.565 | **.004*** | .552 | **.008** | VIIB | -.446 | **.029** | -.579 | **.006** | VIII | -0.431 | **.045** | -0.399 | 0.056 |

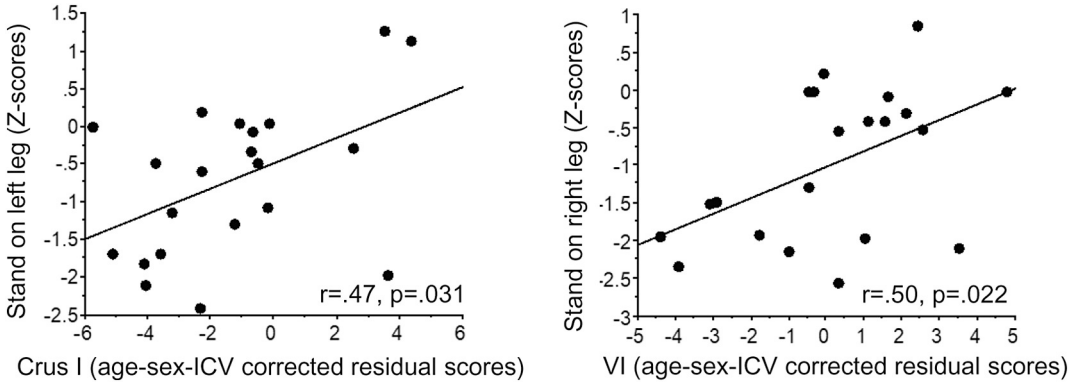


**Fig. 3.** Correlations between ataxia scores and Ceres-based cerebellar lobular volumes of gray matter (residual scores in cc adjusted for age, sex, and ICV).

regional cortical volume declines accelerate in alcoholic participants compared with unaffected controls (Pfefferbaum et al., 2018b; Sullivan et al., 2018). Although the current cross-sectional study did not find age-alcoholism interactions in regional cerebellar volumes, a suggestion of the relevance of drinking age was forthcoming with all three methods in the negative relations observed between older age at AUD onset and smaller volumes of lobule I-V, VIIB, VIII, and Crus II, regions implicated in studies of normal aging (e.g., Persson et al., 2014; Raz et al., 2010; Ziegler et al., 2012). Thus, consistent with our initial speculation, older alcoholics may have a heightened vulnerability to both age and alcoholism as sources of volume deficits.

Our second hypothesis predicted that performance on ataxia tests would correlate with lobular volumes. Several correlations, albeit modest, suggested such relations, where greater static postural instability with eyes open correlated with smaller VI volumes with all three parcellation methods; additional correlations were identified with Ceres in Crus I and SUIT in lobule X. These relations, while convergent, are only suggestive and require replication with larger samples that would also allow for testing sex differences. For example, some studies found that alcoholic men exhibited greater postural instability than alcoholic women (but see Smith and Fein, 2011; Sullivan et al., 2006, 2010) and were more affected by engagement in a secondary cognitive task while attempting to stand still (Sullivan et al., 2015).

A third aim of this study was exploratory and sought relations between hematological indices of nutrition and liver function and lobular volumes. As observed with the ataxia correlations, the most consistent

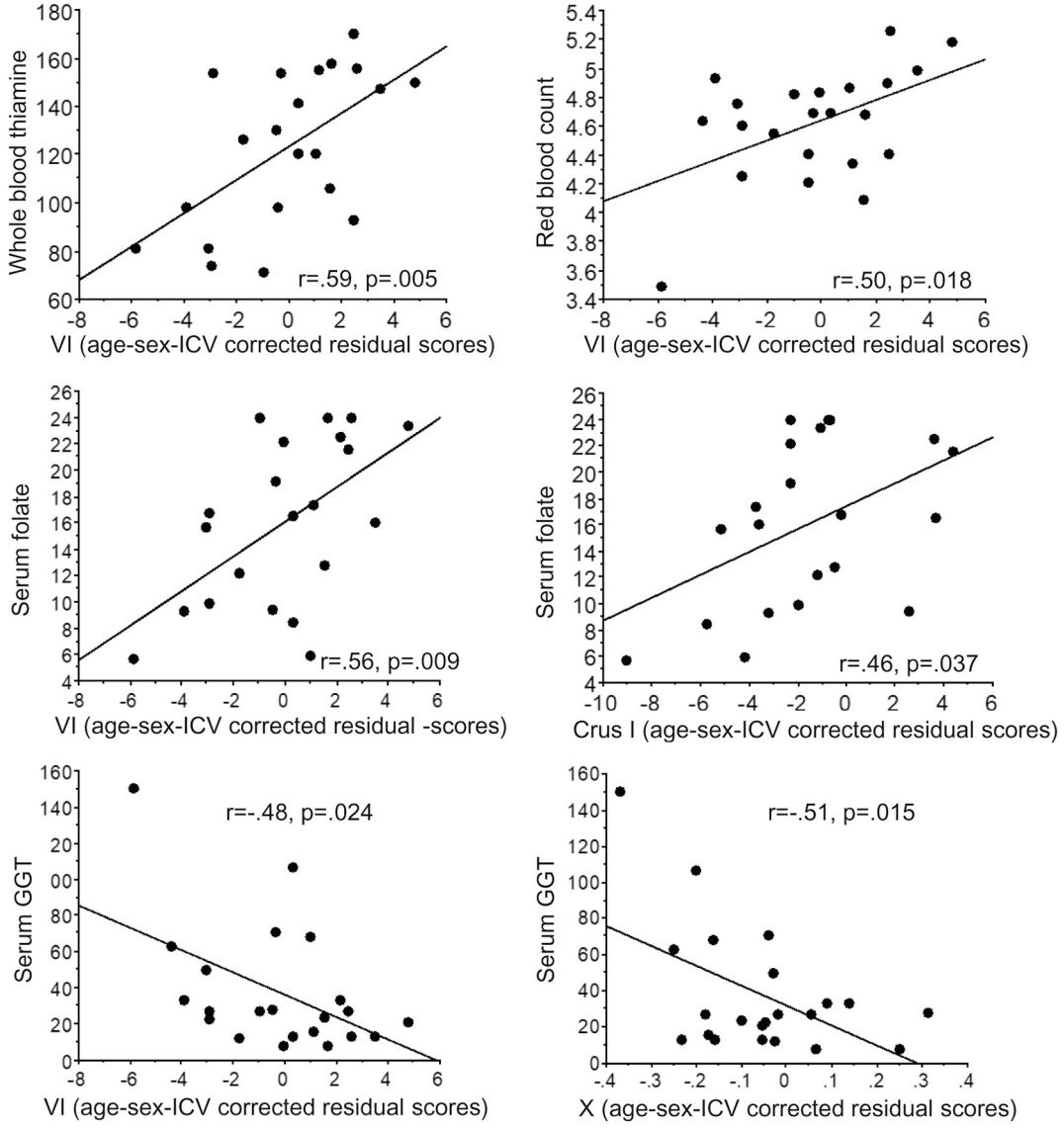


**Fig. 4.** Correlations between hematological indices of nutrition and Ceres-based cerebellar lobular volumes of gray matter (residual scores in cc adjusted for age, sex, and ICV).

relations across the three quantification methods occurred with lobule VI volumes. Lower values of two essential vitamins—thiamine (vitamin B1) and folate (vitamin B9)—along with lower red blood cell count, which are dependent on adequate levels of the B vitamins, correlated with smaller gray matter volumes of VI (all three methods) and Crus I (Ceres only). Although not causative, these relations comport with similar findings reported in the cortical gray matter volumes of recently abstinent alcoholics (Chen et al., 2012; Pfefferbaum et al., 2004). In

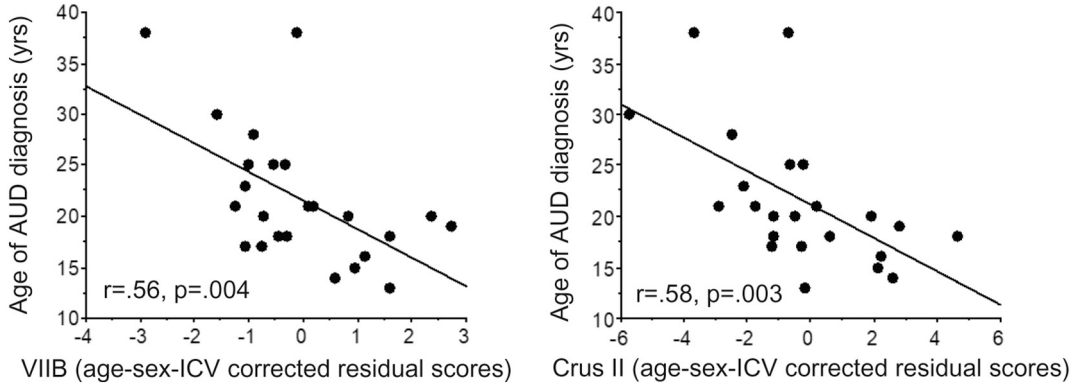


**Fig. 5.** Correlations between age at onset of AUD diagnosis and Ceres-based cerebellar lobular volumes of gray matter (residual scores in cc adjusted for age, sex, and ICV).

complement to the nutritional-cerebellar volume relations, higher GGT levels, possibly reflecting compromised liver function, were correlated with smaller volumes of lobules VI and X using Ceres and SUIT). Again such relations have been reported for cortical volumes (Chen et al., 2012) and may now be extended to regional cerebellar gray matter.

## 5. Limitations

Obvious study limitations include small sample size, restricted age range, and the cross-sectional approach to study a dynamic disorder. The group differences observed were modest but were convergent on several lobules. Further, the brain structure-function relations tested were exploratory and also weak; nonetheless, all reported correlations based on the Ceres cerebellar quantification met FDR correction for multiple comparisons and hold promise for identifying functional relevance of focal cerebellar dysmorphology in neuropsychiatric conditions, including AUD. The imperfect convergence of results across the three quantification methods despite image acquisition with high-resolution data indicates the need for further segmentation refinement and atlas boundary coordination and nomenclature.

## 6. Conclusions

The possibility of quantifying the volume individual cerebellar lobules provides the basis for devising studies to test selective circuitry using multimodal neuroimaging with structural MRI [as attempted herein and (Guell et al., 2019; Guell et al., 2018)], diffusion tensor imaging to identify structural connections between hypothesized neural nodes (e.g., Sullivan et al., 2015), and resting-state functional MRI to seek functional correlated activity between brain regions and structures (e.g., Habas et al., 2009; Krienen and Buckner, 2009). Clearly, all three cerebellar quantification methods examined herein produced similar patterns of group differences and relations with performance and biological data, suggesting that any of the three methods may be used in human studies to seek diagnostic effects or functional correlates of regional cerebellar gray matter volumes. An exemplary impetus for exploring a selective projection in humans comes from a triad of novel studies. The first used optogenetic stimulation in mice and revealed a monosynaptic projection from the dentate nucleus of the cerebellum to the ventral tegmental area (VTA), implicated in rewarding features of addiction and control of social behavior (Carta et al., 2019). Consistent with this newly identified structural circuitry, a second study used resting-state fMRI in healthy young adults and identified a functional network involving cerebellum (dentate nuclei, VIIA, and VI), posterior insula, parietal sensory cortex, and amygdala, possibly contributing to emotional and motivational integration (Habas, 2018). The third study used a primate model and rabies virus labeling, which revealed that lobules VB-VIIIB of the vermis receive dense input from primary motor cortex, suggesting a cortico-cerebellar regulation of gait and posture (Coffman et al., 2011). Together, this set of studies provides directive justification for testing selective cerebellar lobule relations in normal human development and the extent to which each may be disrupted by aging, alcoholism, or other neuropsychiatric conditions.

## Acknowledgment

This research was supported by grants from the National Institute on Alcohol Abuse and Alcoholism (AA010723, AA005965, AA013521, AA023482).

## Declaration of Competing Interest

All authors contributed significantly to this research project, and none has any conflict with this work. This work is not being considered for publication elsewhere.

## Appendix A. Supplementary data

Supplementary data to this article can be found online at https://doi.org/10.1016/j.nicl.2019.101974.

## References

Angelaki, D.E., Yakusheva, T.A., Green, A.M., Dickman, J.D., Blazquez, P.M., 2010. Computation of egomotion in the macaque cerebellar vermis. Cerebellum 9, 174–182.
Baker, K., Harding, A., Halliday, G., Kril, J., Harper, C., 1999. Neuronal loss in functional zones of the cerebellum of chronic alcoholics with and without Wernicke's encephalopathy. Neuroscience 91, 429–438.
Breslow, R.A., Castle, I.P., Chen, C.M., Graubard, B.I., 2017. Trends in alcohol consumption among older Americans: National Health Interview Surveys, 1997 to 2014. Alcohol. Clin. Exp. Res. 41, 976–986.
Carass, A., Cuzzocreo, J.L., Han, S., Hernandez-Castillo, C.R., Rasser, P.E., Ganz, M., Beliveau, V., Dolz, J., Ben Ayed, I., Desrosiers, C., Thyreau, B., Romero, J.E., Coupe, P., Manjon, J.V., Fonov, V.S., Collins, D.L., Ying, S.H., Onyike, C.U., Crocetti, D., Landman, B.A., Mostofsky, S.H., Thompson, P.M., Prince, J.L., 2018. Comparing fully automated state-of-the-art cerebellum parcellation from magnetic resonance images. Neuroimage 183, 150–172.
Carta, I., Chen, C.H., Schott, A.L., Dorizan, S., Khodakhah, K., 2019. Cerebellar modulation of the reward circuitry and social behavior. Science 363.
Chakravarty, M.M., Steadman, P., van Eede, M.C., Calcott, R.D., Gu, V., Shaw, P., Raznahan, A., Collins, D.L., Lerch, J.P., 2013. Performing label-fusion-based segmentation using multiple automatically generated templates. Hum. Brain Mapp. 34, 2635–2654.
Chanraud, S., Pitel, A.L., Rohlfing, T., Pfefferbaum, A., Sullivan, E.V., 2010. Dual tasking and working memory in alcoholism: relation to frontocerebellar circuitry. Neuropsychopharmacology 35, 1868–1878.
Chen, C.H., Walker, J., Momenan, R., Rawlings, R., Heilig, M., Hommer, D.W., 2012. Relationship between liver function and brain shrinkage in patients with alcohol dependence. Alcohol. Clin. Exp. Res. 36, 625–632.
Coffman, K.A., Dum, R.P., Strick, P.L., 2011. Cerebellar vermis is a target of projections from the motor areas in the cerebral cortex. Proc. Natl. Acad. Sci. U. S. A. 108, 16068–16073.
Coupe, P., Yger, P., Prima, S., Hellier, P., Kervrann, C., Barillot, C., 2008. An optimized blockwise nonlocal means denoising filter for 3-D magnetic resonance images. IEEE Trans. Med. Imaging 27, 425–441.
de la Monte, S.M., Tong, M., 2014. Brain metabolic dysfunction at the core of Alzheimer's disease. Biochem. Pharmacol. 88, 548–559.
Desmond, J.E., Chen, S.H., DeRosa, E., Pryor, M.R., Pfefferbaum, A., Sullivan, E.V., 2003. Increased frontocerebellar activation in alcoholics during verbal working memory: an fMRI study. Neuroimage 19, 1510–1520.
Diedrichsen, J., Balsters, J.H., Flavell, J., Cussans, E., Ramnani, N., 2009. A probabilistic MR atlas of the human cerebellum. Neuroimage 46, 39–46.
Fischl, B., Salat, D.H., Busa, E., Albert, M., Dieterich, M., Haselgrove, C., van der Kouwe, A., Killiany, R., Kennedy, D., Klaveness, S., Montillo, A., Makris, N., Rosen, B., Dale, A.M., 2002. Whole brain segmentation: automated labeling of neuroanatomical structures in the human brain. Neuron 33, 341–355.
Fregly, A.R., Graybiel, A., Smith, M.J., 1972. Walk on floor eyes closed (WOFEC): a new addition to an ataxia test battery. Aerosp. Med. 43, 395–399.
Guell, X., Schmahmann, J.D., Gabrieli, J., Ghosh, S.S., 2018. Functional gradients of the cerebellum. Elife 7.
Guell, X., Goncalves, M., Kaczmarzyk, J.R., Gabrieli, J.D.E., Schmahmann, J.D., Ghosh, S.S., 2019. LittleBrain: a gradient-based tool for the topographical interpretation of cerebellar neuroimaging findings. PLoS One 14, e0210028.
Habas, C., 2018. Research note: a resting-state, cerebello-amygdaloid intrinsically connected network. Cerebellum Ataxias 5, 4.
Habas, C., Kamdar, N., Nguyen, D., Prater, K., Beckmann, C.F., Menon, V., Greicius, M.D., 2009. Distinct cerebellar contributions to intrinsic connectivity networks. J. Neurosci. 29, 8586–8594.
Klein, A., Andersson, J., Ardekani, B.A., Ashburner, J., Avants, B., Chiang, M.C., Christensen, G.E., Collins, D.L., Gee, J., Hellier, P., Song, J.H., Jenkinson, M., Lepage, C., Rueckert, D., Thompson, P., Vercauteren, T., Woods, R.P., Mann, J.J., Parsey, R.V., 2009. Evaluation of 14 nonlinear deformation algorithms applied to human brain MRI registration. Neuroimage 46, 786–802.
Koeppen, A.H., 2018. The neuropathology of the adult cerebellum. Handb. Clin. Neurol. 154, 129–149.
Krienen, F.M., Buckner, R.L., 2009. Segregated fronto-cerebellar circuits revealed by intrinsic functional connectivity. Cereb. Cortex 19, 2485–2497.
Le Berre, A.P., Pitel, A.L., Chanraud, S., Beaunieux, H., Eustache, F., Martinot, J.L., Reynaud, M., Martelli, C., Rohlfing, T., Sullivan, E.V., Pfefferbaum, A., 2014. Chronic alcohol consumption and its effect on nodes of frontocerebellar and limbic circuitry: comparison of effects in France and the United States. Hum. Brain Mapp. 35, 4635–4653.
Manjon, J.V., Coupe, P., 2016. volBrain: an online MRI brain volumetry system. Front. Neuroinform. 10, 30.
Mathalon, D.H., Sullivan, E.V., Rawles, J.M., Pfefferbaum, A., 1993. Correction for head size in brain-imaging measurements. Psychiatry Res. Neuroimaging 50, 121–139.
Monnig, M.A., Caprihan, A., Yeo, R.A., Gasparovic, C., Ruhl, D.A., Lysne, P., Bogenschutz, M.P., Hutchison, K.E., Thoma, R.J., 2013. Diffusion tensor imaging of white matter networks in individuals with current and remitted alcohol use disorders and

comorbid conditions. Psychol. Addict. Behav. 27, 455–465.
Mosconi, M.W., Wang, Z., Schmitt, L.M., Tsai, P., Sweeney, J.A., 2015. The role of cerebellar circuitry alterations in the pathophysiology of autism spectrum disorders. Front. Neurosci. 9, 296.
Nadkarni, N.K., Nunley, K.A., Aizenstein, H., Harris, T.B., Yaffe, K., Satterfield, S., Newman, A.B., Rosano, C., Health, A.B.C.S., 2014. Association between cerebellar gray matter volumes, gait speed, and information-processing ability in older adults enrolled in the Health ABC study. J. Gerontol. A Biol. Sci. Med. Sci. 69, 996–1003.
Nakamura-Palacios, E.M., Souza, R.S., Zago-Gomes, M.P., de Melo, A.M., Braga, F.S., Kubo, T.T., Gasparetto, E.L., 2014. Gray matter volume in left rostral middle frontal and left cerebellar cortices predicts frontal executive performance in alcoholic subjects. Alcohol. Clin. Exp. Res. 38, 1126–1133.
Nasreddine, Z.S., Phillips, N.A., Bedirian, V., Charbonneau, S., Whitehead, V., Collin, I., Cummings, J.L., Chertkow, H., 2005. The montreal cognitive assessment, MoCA: a brief screening tool for mild cognitive impairment. J. Am. Geriatr. Soc. 53, 695–699.
Park, M.T., Pipitone, J., Baer, L.H., Winterburn, J.L., Shah, Y., Chavez, S., Schira, M.M., Lobaugh, N.J., Lerch, J.P., Voineskos, A.N., Chakravarty, M.M., 2014. Derivation of high-resolution MRI atlases of the human cerebellum at 3T and segmentation using multiple automatically generated templates. Neuroimage 95, 217–231.
Persson, N., Ghisletta, P., Dahle, C.L., Bender, A.R., Yang, Y., Yuan, P., Daugherty, A.M., Raz, N., 2014. Regional brain shrinkage over two years: individual differences and effects of pro-inflammatory genetic polymorphisms. Neuroimage 103, 334–348.
Pfefferbaum, A., Lim, K.O., Zipursky, R.B., Mathalon, D.H., Lane, B., Ha, C.N., Rosenbloom, M.J., Sullivan, E.V., 1992. Brain gray and white matter volume loss accelerates with aging in chronic alcoholics: a quantitative MRI study. Alcohol. Clin. Exp. Res. 16, 1078–1089.
Pfefferbaum, A., Rosenbloom, M.J., Serventi, K.L., Sullivan, E.V., 2004. Brain volumes, RBC status, and hepatic function in alcoholics after 1 and 4 weeks of sobriety: predictors of outcome. Am. J. Psychiatry 161, 1190–1196.
Pfefferbaum, A., Kwon, D., Brumback, T., Thompson, W.K., Cummins, K., Tapert, S.F., Brown, S.A., Colrain, I.M., Baker, F.C., Prouty, D., De Bellis, M.D., Clark, D.B., Nagel, B.J., Chu, W., Park, S.H., Pohl, K.M., Sullivan, E.V., 2018a. Altered brain developmental trajectories in adolescents after initiating drinking. Am. J. Psychiatry 175, 370–380.
Pfefferbaum, A., Zahr, N.M., Sassoon, S.A., Kwon, D., Pohl, K.M., Sullivan, E.V., 2018b. Accelerated and premature aging characterizing regional cortical volume loss in human immunodeficiency virus infection: contributions from alcohol, substance use, and hepatitis C coinfection. Biol. Psychiatry Cogn. Neurosci. Neuroimag. 3, 844–859.
Phillips, S.C., Harper, C.G., Kril, J., 1987. A quantitative histological study of the cerebellar vermis in alcoholic patients. Brain 110, 301–314.
Price, M., Cardenas, V.A., Fein, G., 2014. Automated MRI cerebellar size measurements using active appearance modeling. Neuroimage 103, 511–521.
Raz, N., Dupuis, J.H., Briggs, S.D., McGavran, C., Acker, J.D., 1998. Differential effects of age and sex on the cerebellar hemispheres and the vermis: a prospective MR study. AJNR Am. J. Neuroradiol. 19, 65–71.
Raz, N., Ghisletta, P., Rodrigue, K.M., Kennedy, K.M., Lindenberger, U., 2010. Trajectories of brain aging in middle-aged and older adults: regional and individual differences. Neuroimage 51, 501–511.
Rindi, G., Patrini, C., Comincioli, V., Reggiani, C., 1980. Thiamine content and turnover rates of some rat nervous regions, using labeled thiamine as a tracer. Brain Res. 181, 369–380.
Ritz, L., Coulbault, L., Lannuzel, C., Boudehent, C., Segobin, S., Eustache, F., Vabret, F., Pitel, A.L., Beaunieux, H., 2016. Clinical and biological risk factors for neuropsychological impairment in alcohol use disorder. PLoS One 11, e0159616.
Rohlfing, T., Maurer, C.R., 2003. Nonrigid image registration in shared-memory multiprocessor environments with application to brains, breasts, and bees. IEEE Trans. Inf. Technol. Biomed. 7, 16–25.
Rohlfing, T., Zahr, N.M., Sullivan, E.V., Pfefferbaum, A., 2010. The SRI24 multi-channel atlas of normal adult human brain structure. Hum. Brain Mapp. 31, 798–819.
Romero, J.E., Coupe, P., Giraud, R., Ta, V.T., Fonov, V., Park, M.T.M., Chakravarty, M.M., Voineskos, A.N., Manjon, J.V., 2017. CERES: a new cerebellum lobule segmentation method. Neuroimage 147, 916–924.
Sawyer, K.S., Oscar-Berman, M., Mosher Ruiz, S., Galvez, D.A., Makris, N., Harris, G.J., Valera, E.M., 2016. Associations between cerebellar subregional morphometry and alcoholism history in men and women. Alcohol. Clin. Exp. Res. 40, 1262–1272.
Schmahmann, J.D., 2019. The cerebellum and cognition. Neurosci. Lett. 688, 62–75.
Smith, S., 2002. Fast robust automated brain extraction. Hum. Brain Mapp. 17, 143–155.
Smith, S., Fein, G., 2011. Persistent but less severe ataxia in long-term versus short-term abstinent alcoholic men and women: a cross-sectional analysis. Alcohol. Clin. Exp. Res. 35, 2184–2192.
Stoodley, C.J., Valera, E.M., Schmahmann, J.D., 2012. Functional topography of the cerebellum for motor and cognitive tasks: an fMRI study. Neuroimage 59, 1560–1570.
Stoodley, C.J., MacMore, J.P., Makris, N., Sherman, J.C., Schmahmann, J.D., 2016. Location of lesion determines motor vs. cognitive consequences in patients with cerebellar stroke. Neuroimage Clin. 12, 765–775.
Sullivan, E.V., 2003. Compromised pontocerebellar and cerebellothalamocortical systems: speculations on their contributions to cognitive and motor impairment in nonamnesic alcoholism. Alcohol. Clin. Exp. Res. 27, 1409–1419.
Sullivan, E.V., Deshmukh, A., Desmond, J.E., Lim, K.O., Pfefferbaum, A., 2000. Cerebellar volume decline in normal aging, alcoholism, and Korsakoff's syndrome: relation to ataxia. Neuropsychology 14, 341–352.
Sullivan, E.V., Harding, A.J., Pentney, R., Dlugos, C., Martin, P.R., Parks, M.H., Desmond, J.E., Chen, S.H., Pryor, M.R., De Rosa, E., Pfefferbaum, A., 2003. Disruption of frontocerebellar circuitry and function in alcoholism. Alcohol. Clin. Exp. Res. 27, 301–309.
Sullivan, E.V., Rose, J., Pfefferbaum, A., 2006. Effect of vision, touch and stance on cerebellar vermian-related sway and tremor: a quantitative physiological and MRI study. Cereb. Cortex 16, 1077–1086.
Sullivan, E.V., Rose, J., Pfefferbaum, A., 2010. Physiological and focal cerebellar substrates of abnormal postural sway and tremor in alcoholic women. Biol. Psychiatry 67, 44–51.
Sullivan, E.V., Zahr, N.M., Rohlfing, T., Pfefferbaum, A., 2015. Cognitive demands during quiet standing elicit truncal tremor in two frequency bands: differential relations to tissue integrity of corticospinal tracts and cortical targets. Front. Hum. Neurosci. 9, 175.
Sullivan, E.V., Zahr, N.M., Sassoon, S.A., Thompson, W.K., Kwon, D., Pohl, K.M., Pfefferbaum, A., 2018. The role of aging, drug dependence, and hepatitis C comorbidity in alcoholism cortical compromise. JAMA Psychiatry 75, 474–483.
Sutherland, G.T., Sheedy, D., Kril, J.J., 2014. Neuropathology of alcoholism. Handb. Clin. Neurol. 125, 603–615.
Torvik, A., Torp, S., 1986. The prevalence of alcoholic cerebellar atrophy: A morphometric and histological study of an autopsy material. J. Neurol. Sci. 75, 43–51.
Tustison, N.J., Avants, B.B., Siqueira, M., Gee, J.C., 2011. Topological well-composedness and glamorous glue: a digital gluing algorithm for topologically constrained front propagation. IEEE Trans. Image Process. 20, 1756–1761.
Victor, M., Adams, R.D., Collins, G.H., 1989. The Wernicke-Korsakoff Syndrome and Related Neurologic Disorders Due to Alcoholism and Malnutrition, 2nd edition. F.A. Davis Co, Philadelphia.
Wechsler, D., 2001. Wechsler Test of Adult Reading (WTAR). Pearson Education, Inc, San Antonio, TX.
Weier, K., Fonov, V., Lavoie, K., Doyon, J., Collins, D.L., 2014. Rapid automatic segmentation of the human cerebellum and its lobules (RASCAL)–implementation and application of the patch-based label-fusion technique with a template library to segment the human cerebellum. Hum. Brain Mapp. 35, 5026–5039.
Yang, Z., Ye, C., Bogovic, J.A., Carass, A., Jedynak, B.M., Ying, S.H., Prince, J.L., 2016. Automated cerebellar lobule segmentation with application to cerebellar structural analysis in cerebellar disease. Neuroimage 127, 435–444.
Yu, T., Korgaonkar, M.S., Grieve, S.M., 2017. Gray matter atrophy in the cerebellum-evidence of increased vulnerability of the crus and vermis with advancing age. Cerebellum 16, 388–397.
Zahr, N.M., Pfefferbaum, A., 2017. Alcohol's effects on the brain: neuroimaging results in humans and animal models. Alcohol Res. Health 38, 183–206.
Zahr, N.M., Pohl, K.M., Saranathan, M., Sullivan, E.V., Pfefferbaum, A., 2019. Hippocampal subfield CA2+3 exhibits accelerated aging in alcohol use disorder: a preliminary study. Neuroimage 22, 101764.
Zhao, Q., Pfefferbaum, A., Podhajsky, S., Pohl, K.M., Sullivan, E.V., 2019. Accelerated aging and motor control deficits are related toregional deformation of central cerebellar white matter inalcohol use disorder. Addict. Biol. 1–12.
Ziegler, G., Dahnke, R., Jancke, L., Yotter, R.A., May, A., Gaser, C., 2012. Brain structural trajectories over the adult lifespan. Hum. Brain Mapp. 33, 2377–2389.